16th World Conference on Earthquake Engineering, 16WCEE 2017
Santiago Chile, January 9th to 13th 2017
Paper N° 1276
Registration Code: S-C1463150657

HYSTERETIC PERFORMANCE OF NEW GENERATION BUCKLING RESTRAINED BRACES

W. Xu[(1)], C.P. Pantelides[(2)], K. Robinson[(3)], S.D. Powell[(4)]

[(1)] *Ph.D. Candidate, Department of Civil and Env. Eng., Univ. of Utah, Salt Lake City, USA, wenjing.xu@utah.edu*
[(2)] *Professor, Department of Civil and Env. Eng., Univ. of Utah, Salt Lake City, USA, c.pantelides@utah.edu*
[(3)] *Engineer, Corebrace, Salt Lake City, USA, kim.robinson@corebrace.com*
[(4)] *Vice Pesident, Corebrace, Salt Lake City, USA, steve.powell@corebrace.com*

Abstract
The performance of a new type of Buckling Restrained Braces (BRBs) is described in this research. These BRBs offer advantages since the steel core is composed of straight steel plates with connection plates welded perpendicular to the steel core; this is different from conventional BRB designs in which the steel core plates are continuous with the connection plates. Since the steel core plate is prismatic, construction of the new type of BRBs saves steel material and reduces manufacturing costs. Four full-scale BRBs using a prismatic steel core were tested under quasi-static cyclic load with either a single core plate or dual core plates, and connection plates either bolted or welded to gussets. In the full-scale experiments, the ratio of maximum compression to maximum tension ranged between 1.06 and 1.25 and the cumulative inelastic deformation was 2.1 to 3.1 times higher than American Institute of Steel Construction (AISC) requirements. The hysteresis curves exhibited stable, repeatable behavior with positive incremental stiffness. There was no rupture, instability, or end-connection failure for deformations up to 2% story drift; at failure, the steel core plates achieved strains between 3.2 and 4.2%. The performance of the new BRBs was comparable to conventional BRBs in terms of cumulative hysteretic energy dissipation. Buckling of the steel core plates in either the strong-axis or weak-axis was observed in the experiments. The strong-axis and weak-axis buckling behavior was analyzed using strut-and-tie models. Bulging of the steel casing was observed in some of the experiments. The bulging behavior is idealized as a local buckling phenomenon using plastic analysis models for strong-axis or weak-axis buckling. In this paper, a model is proposed for determining the potential for bulging when strong-axis buckling occurs.

Keywords: BRB; connection plates; strong-axis buckling; weak-axis buckling; bulging.

1. Introduction

Buckling Restrained Braces (BRBs) are used in buildings to dissipate energy in earthquakes. Use of BRBs has expanded since the 1994 Northbridge Earthquake; BRBs are becoming popular in damage control designs [1, 2]. BRBs consist of a steel casing housing one or more steel core plates, surrounded by concrete with a gap in-between the steel core and concrete. A significant amount of research has been carried out regarding experimental performance of BRBs [3-9], and the configuration of the BRB cross-section. General BRB cross-sectional configurations include: rectangular core plate restrained by a round or rectangular steel casing filled with concrete [10-12]; rectangular core plate restrained by two steel tubes [13]; cylinder-shaped core plate in a round or rectangular steel casing [14]; H-shaped core plate restrained by a steel casing [15]; rectangular core plate restrained by metal plates bolted together as the casing [16]; H-shaped steel section [17]; and cruciform core plate restrained by concrete and steel casing [3, 18, 19]. Once the steel core buckles under cyclic compression in either the strong-axis or the weak-axis, the steel core comes into contact with the concrete inside the steel casing; under certain conditions, the contact forces between the steel core and concrete cause bulging of the casing. Research regarding the contact force between core and casing has been performed [20, 21]. In addition, research has been performed regarding the local buckling restraint condition and local bulging of the steel casing [20, 22-26].

In many BRB types the steel core also serves as the connection plate. In current BRB configurations, the connection plate and steel core are manufactured from a single steel plate formed by reducing the cross-section's width, as shown in Fig. 1(a). Manufacturing of the core for current BRB configurations wastes steel material and requires skilled labor and special machinery. BRBs with a new configuration of steel core and connection plates were developed to reduce manufacturing and material costs. The connection plates are welded perpendicular to a prismatic steel core, as shown in Fig. 1(b). There is no cutting of the core, and assembly is easier since the presence of two connection plates at each BRB end, facilitates the assembly of pinned, bolted, and welded connections.

Seismic provisions for structural steel buildings stipulate specific criteria that BRBs must satisfy for acceptable performance [27]; these include compression strength and strain hardening adjustment factors, cumulative inelastic deformation, and cumulative energy dissipation. This paper focuses on describing the details, experimental behavior, and performance of four new BRBs tested in full-scale experiments. Strong-axis and weak-axis core plate buckling and bulging of the steel casing are described and analyzed.

2. Experimental Investigation

Four new BRBs were tested in full-scale experiments; the characteristics of the specimens are summarized in Table 1; W_{co} is the width of the core plates, A_{co} is the cross-sectional area of the core, $L_{c\text{-}co}$ is the critical length of the core, and L_{tot} is the total length of the BRB. All BRBs had a square casing with core plates ranging in width from 197 to 254 mm. The outside cross-sectional dimensions of the casing were either 305 x 305 mm or 254 x 254 mm; the steel casing wall was 6 mm thick. Two of the BRBs had dual core plates and the other two had a single core plate; the thickness of a single core plate was 25 mm. The material properties of all core plates were: yield stress of 281 MPa and ultimate strength of 412 MPa. Three BRBs had a length of 5.56 m and one 5.31 m. The side view of a typical BRB is shown in Fig. 2. The yielding portion of the core plate is the section between the connection plates in the longitudinal direction, denoted as $L_{c\text{-}co}$ in Fig. 2.

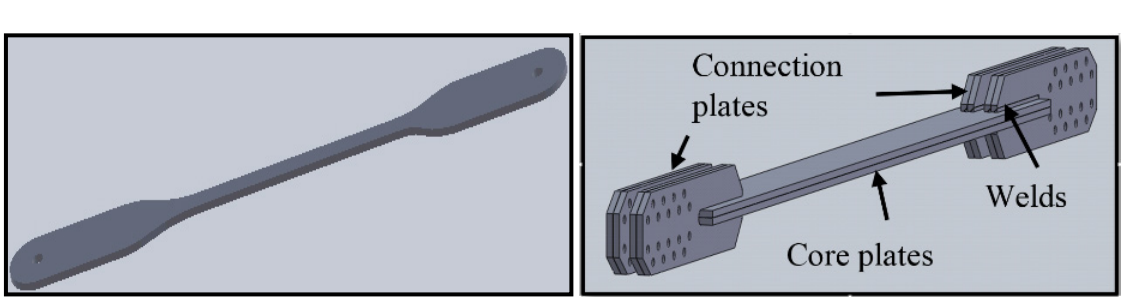

(a) (b)

Fig. 1 - Steel core and connection plates: (a) conventional BRBs; (b) new generation BRBs

Each BRB was assembled in the load frame vertically, as shown in Fig. 3. The top gusset plate was attached to a hydraulic actuator with an inline load cell and the bottom gusset was fixed to the ground. The boundary and loading conditions for each specimen are listed in Table 1. Two BRBs were tested with axial cyclic load only (F); the other two BRBs were tested with axial cyclic load and initial momento (FM). Three of the BRBs were assembled to the gusset plates with bolts and one was welded.

Table 1 - Test type, boundary condition, material properties, and specimen geometry

Test #	Loading condition	End connection	W_{co} (mm)	Core type	A_{co} (mm^2)	$L_{c\text{-}co}$ (mm)	L_{tot} (mm)	Casing (mmxmmxmm)
1	F	Bolted	235	Dual	11935	3124	5563	305x305x6.4
2	F	Bolted	159	Dual	8065	3429	5309	305x305x6.4
3	FM	Welded	254	Single	6452	3886	5563	305x305x6.4
4	FM	Bolted	197	Single	5000	3988	5563	254x254x6.4

Note: F = Force; FM = Force and initial moment

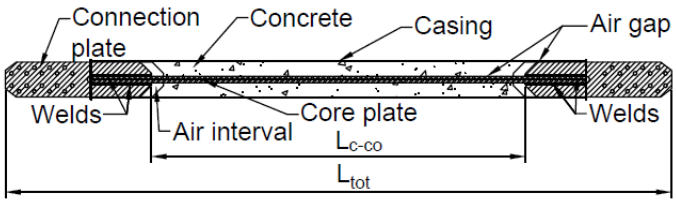

Fig. 2 - Side view of BRB

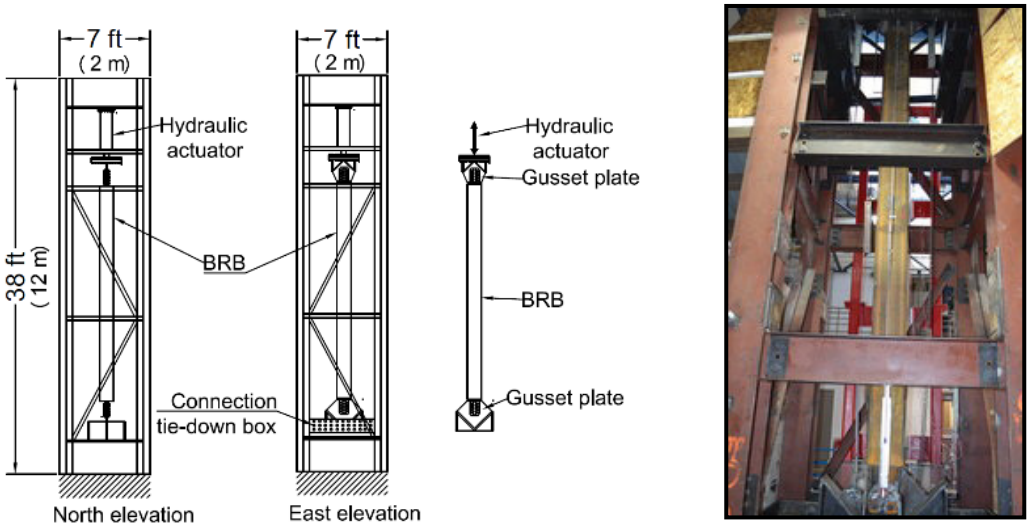

Fig. 3 - Test frame and elevation

3. Evaluation of BRB performance

Acceptance criteria for BRB performance include stability of the hysteresis loops, compression strength and strain hardening adjustment factors, cumulative inelastic deformation, and cumulative hysteretic energy dissipation [27]. The BRBs tested in this research demonstrated a variety of failures. A summary of these phenomena is provided in Table 2. BRBs in tests 1, 3 and 4 had strong-axis buckling and the BRB in test 2 had weak-axis buckling. The buckling deformations of the core plates after the tests were carried out are shown in Fig. 4. Fig. 5 shows the hysteresis loops which are stable up to a displacement corresponding to 2% story drift; there is no fracture and drift capacity meets AISC 341 requirements [27]. The maximum strain in the core plates ranged from 3.2 to 4.2%, as shown in Table 3.

Table 2 - Failure modes of new generation BRB specimens

Test #	Description of failure	Buckling direction
1	Fracture of core plate at two ends/casing bulging at mid-height	ST
2	Buckling of core plate	W
3	Buckling of core plate	ST
4	Tension/core plate fracture at mid-height	ST

Note: W = weak-axis; ST = strong-axis

(a) (b) (c) (d)

Fig. 4 - Failure modes observed in BRB tests: (a) #1; (b) #2; (c) #3; (d) #4

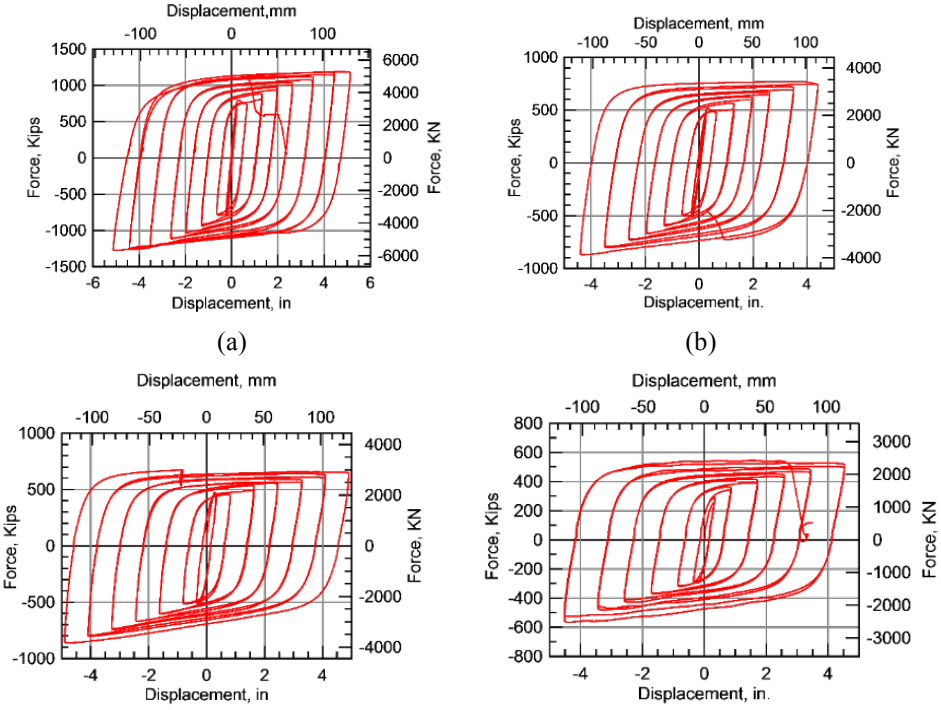

(a) (b)

(c) (d)

Fig. 5 - Hysteresis behavior of new BRBs: (a) #1; (b) #2; (c) #3; (d) #4

Table 3 - Performance Parameters of BRB Specimens

Test	Maximum displacement (mm)	Final cycle	Maximum strain (%)	β	ω	η	E (kN-m)
1	130	16	4.16	1.06	1.57	617	12882
2	112	14	3.28	1.11	1.46	471	6500
3	125	13	3.21	1.25	1.61	521	5977
4	132	13	3.30	1.19	1.67	472	5560

3.1 Compression strength adjustment factor

This is defined as the ratio of maximum compressive to maximum tensile force. AISC 341 provisions [27] require this factor to be within certain limits, expressed as:

$$1.00 < \beta = (P_{max}/T_{max}) < 1.30 \quad (1)$$

where β is the compression strength adjustment factor; P_{max} is the maximum compressive force; and T_{max} is the maximum tensile force in the corresponding load cycle. Table 3 shows that values of β vary from 1.06 to 1.25 which meets AISC 341 requirements [27].

3.2 Strain hardening adjustment factor

This factor is defined as the ratio of maximum tension force from tests to measured yield force:

$$\omega = (T_{max} / R_y P_{ysc}) \geq 1.00 \quad (2)$$

where T_{max} is the maximum tensile force, and R_y is the ratio of expected yield stress to specified minimum yield stress, F_y. Factor R_y need not be applied if the axial yield strength of the steel core, P_{ysc}, is established from coupon tests, which is the case here. The displacement applied in the first loading step is the yield displacement. BRBs started strain hardening after the first loading step and all BRBs eventually attained strain hardening in later steps. The maximum value of ω ranged from 1.46 to 1.67.

3.3 Cumulative inelastic deformation

Inelastic deformation for each cycle, μ_i, is the ratio of permanent or plastic BRB axial displacement divided by the length of the yielding portion of the brace. The inelastic deformation for each cycle, μ_i, is expressed as:

$$\mu_i = 2(\Delta_{max\_c} + \Delta_{max\_t}) / \Delta_{by} - 4 \quad (3)$$

where Δ_{max_c} is the maximum displacement of the brace in compression; Δ_{max_t} is the maximum displacement of the brace in tension; and Δ_{by} is the yield displacement of the brace, which is the ratio of the force at yield to the stiffness of the yielding core.

According to AISC 341 provisions the cumulative inelastic axial ductility capacity is obtained as [27]:

$$\eta = \Sigma \mu_i \quad (4)$$

where i is the loading cycle number from 1 to n and n is the final loading cycle at failure. From Table 3, the minimum cumulative inelastic deformation is 472 for test 4 with the small core cross-sectional, and the maximum is 617 for test 1 with the large core cross-sectional area. The four specimens exceeded the AISC 341 cumulative inelastic deformation requirement of 200 times the yield displacement.

3.4 Cumulative hysteretic energy dissipation

Cumulative hysteretic energy dissipation is used to measure the energy dissipated by a BRB. Energy dissipation for each loading increment is obtained as:

$$E_{j+1} = (P_{j+1} + P_j)\,(x_{j+1} - x_j) / 2 \quad (5)$$

where P_j and P_{j+1} are BRB forces at time j and $(j+1)$, respectively; and x_j and x_{j+1} are BRB displacements at time j and $(j+1)$, respectively. Cumulative energy dissipation is the summation of energy for each loading increment, expressed as:

$$E = \Sigma\, E_{j+1} \quad (6)$$

where E_{j+1} is the energy dissipation for each loading increment and E is the cumulative energy dissipation. The summation for j is from 1 to $(n-1)$. Cumulative hysteretic energy dissipation is plotted in Fig. 6(a) and final values are given in Table 3. Cumulative hysteretic energy dissipation for specimens 1, 2 and 3 is higher than that for specimen 4; the larger the cross-sectional area of the core the higher the hysteretic energy dissipated.

4. Comparison of new to conventional BRBs

Raddon et al. [11] reported cyclic test results for a conventional BRB with pinned connections; this BRB had a cross-sectional area of 12258 mm^2 using three steel core plates. The BRB in test 1 had a cross-sectional area of 11935 mm^2 which is 97.4% of the conventional BRB [11]. The cumulative hysteretic energy dissipation for these two tests in Fig. 6(b) shows that new and conventional BRBs dissipated similar amounts of hysteretic energy.

5. Simulation of hysteretic behavior of BRBs using finite elements

A finite element analysis of BRBs tested in this research was carried out using Ansys [28]. Three-dimensional 20-node solid element 186 was used for the steel casing, concrete and steel core plates. A combination of nonlinear kinematic and isotropic hardening was used for the steel core; a linear material property was used for the concrete and steel casing. Finite element models were built for the four tests. The hysteresis loops and cumulative energy dissipation obtained from the finite element simulation are compared with the tests, as shown in Figs. 7 and 8. Finite element simulation results were similar to the test results for both the shape of the hysteresis loops and the hysteretic energy dissipation.

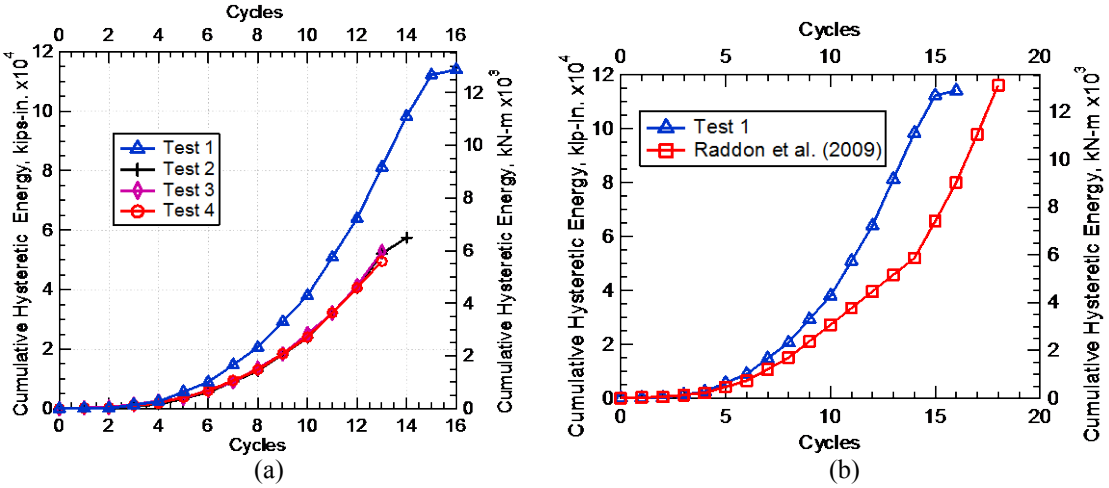

Fig. 6 - Cumulative energy dissipation of BRBs: (a) new BRBs (b) Comparison of of new and conventional BRBs

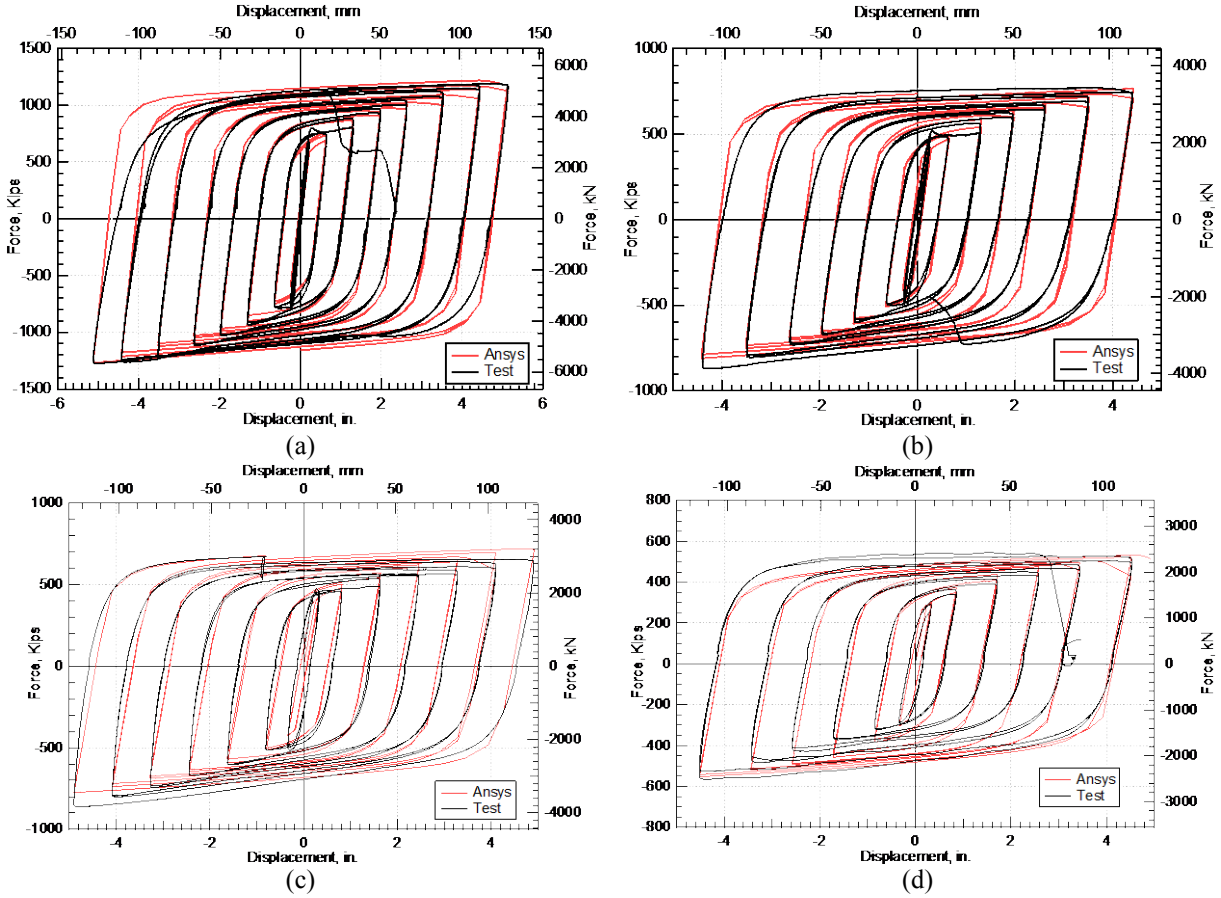

Fig. 7 - Comparison of hysteresis loops for simulation and test results(a) #1; (b) #2; (c) #3; (d) #4

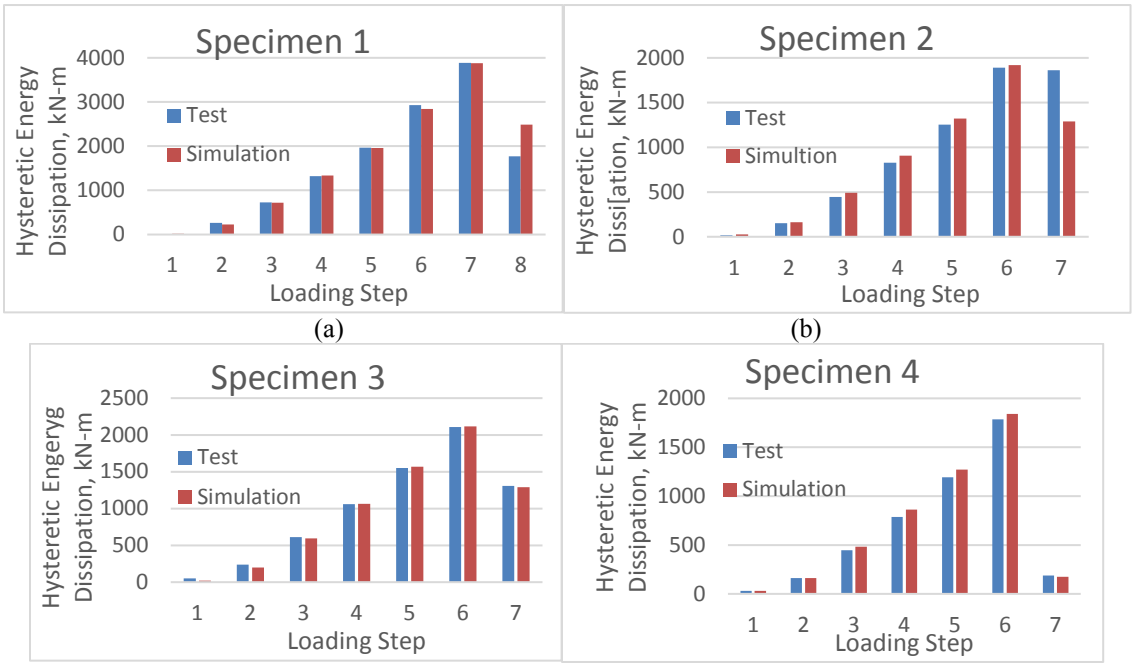

Fig. 8 - Hysteretic energy comparison for the four tests

6. Strong-axis and weak-axis buckling and bulging

In the full-scale tests, core plates buckled in the weak-axis or stong-axis, as summarized in Table 2. Strong-axis buckling was observed in tests 1, 3 and 4, and weak-axis buckling in test 2, as shown in Fig. 4. Buckling occuring in different directions can be explained using the strut-and-tie model (STM) [29]. The STM is a truss idealization of composite members consisting of steel ties and concrete struts and nodes [30].

The ACI 318 building code [29] specifies the minimum angle between a strut and tie as 25º; angle θ needs to be large enough to mitigate cracking and avoid incompatibilities; when this angle is smaller than 25º, the node and strut may crush. Once concrete crushes, the core plates deform in the strong direction before they can deform in the weak direction. When the angle between strut and tie is larger than 25º, the nodes and struts are stable and the core plate buckles in the weak-axis. The BRB cross-section for tests 1 and 2 is shown in Figs. 9(a) and 9(b), respectively. An STM is constructed using the steel casing as the tie, and concrete as the struts and nodes. Angle, θ, between strut and tie in test 1 was 13.3º, which is smaller than 25º; concrete on the side of the core plates crushed and the core plates buckled in the strong-axis. Angle, θ, between strut and tie in test 2 was 28.9º, which is greater than 25º; concrete above the core plates crushed and the core plates experienced weak-axis buckling.

After the steel core buckles, concrete is pushed against the steel casing which deforms or bulges. The contact force is critical for determining whether the steel casing will bulge. Bulging experienced in test 1 was very noticeable and is shown in Fig. 10. Lin et al. [20] defined a demand-to-capacity ratio (DCR) to evaluate local bulging failure of the steel casing for weak axis buckling as:

$$DCR = \frac{P_{max}\left(2w_s - w_{eff}\right)s}{l_w\, l_{eff}\, t_s^2\, f_{ys}} \tag{7}$$

where P_{max} is the maximum compressive force applied on the BRB; w_s is the width of the steel tube; w_{eff} and l_{eff} are the width and length of the effective inner surface, as shown in Fig. 11; s is the air gap thickness between concrete and steel core; l_w is the wavelength; and t_s and f_{ys} are the wall thickness and yield strength of the steel casing, respectively.

Occurence of bulging when strong-axis buckling occurs can be explained using Eq. (7) with appropriate definitions of the width and length of the effective inner surface. For bulging of the casing in strong axis buckling, since the steel core width is significantly larger than the core thickness, contact between the steel core and concrete is assumed as a line contact. ACI 318 [29] recommends that when the supporting area is wider than the loaded area on all sides, the surrounding concrete confines the bearing area, resulting in an increase in bearing strength. The supporting area can be obtained by spreading the loaded area with a ratio of 2:1 (width to depth). Therefore, the width of the effective inner surface is assumed equal to the thickness of the steel core plates plus four times the concrete cover. For strong axis buckling, the experiments and numerical simulations indicate that a contact surface equal to one-third of the core width, $w_c/3$, is appropriate with a spreading slope of 2:1 in both the transverse and longitudinal directions to determine the width and length of the effective area, as shown in Fig. 12. The width and length of the effective inner face are expressed as:

$$w_{eff-s} = t_c + 4c_s \leq w_s \tag{8a}$$

$$l_{eff-s} = w_c/3 + 4c_s \leq l_{w-s} \tag{8b}$$

where, w_{eff-s} and l_{eff-s} are the width and length of the inner effective area for strong-axis buckling of the core plates; t_c is the thickness of the core plates; c_s is the concrete cover thickness in the strong-axis of the core plates; in the case of strong-axis buckling the wavelength is obtained as $l_{w-s} = 5.9\, w_c$ based on previous research [31].

Table 4 lists the DCR for all specimens; P_{max} is the maximum compressive force obtained in the experiments. According to Eqs. (7) and (8), BRBs in Tests 1, 2 and 3 should exhibit bulging of the steel casing, whereas the BRB in Test 4 should not bulge; the DCR values and the outcomes agree with the phenomena observed in the tests.

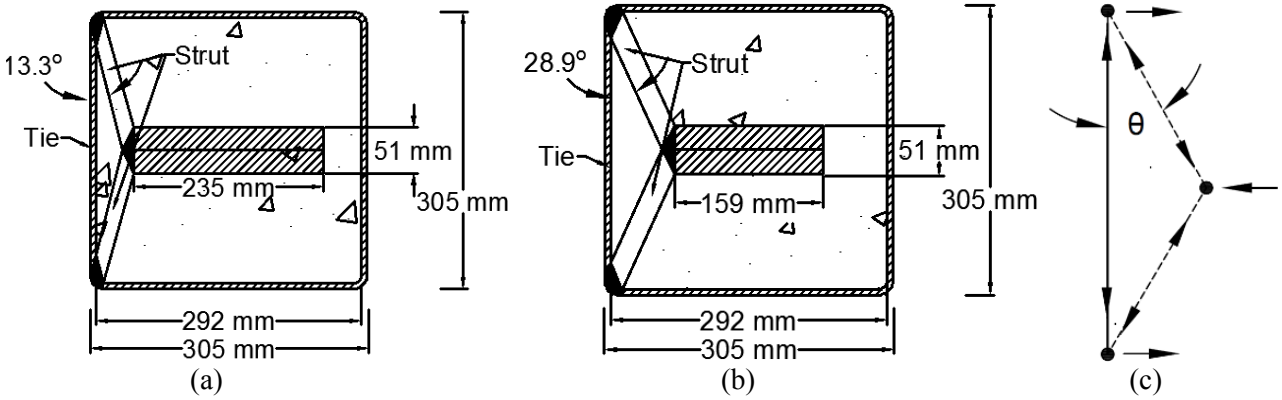

Fig. 9 - Strut-and-tie model for two BRB cross-sections: (a) #1, (b) #2, (c) θ

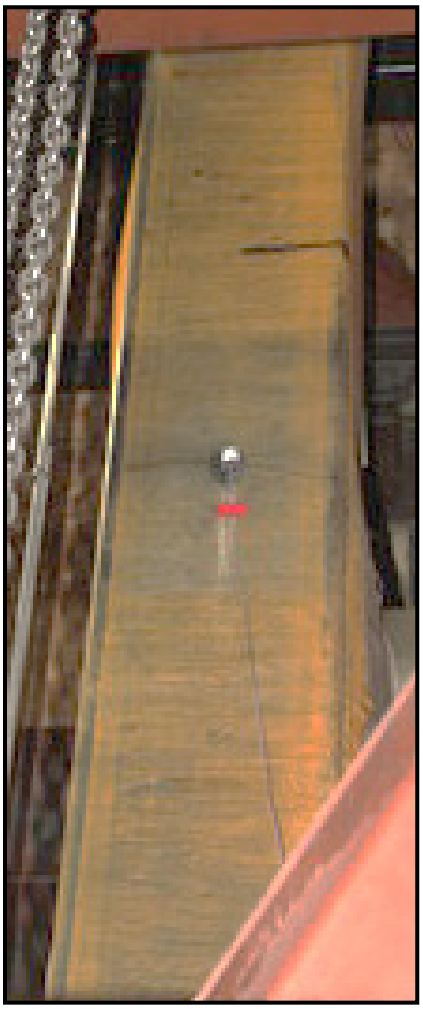

Fig. 10 - Bulging of steel casing in test 1 following strong-axis buckling of the core

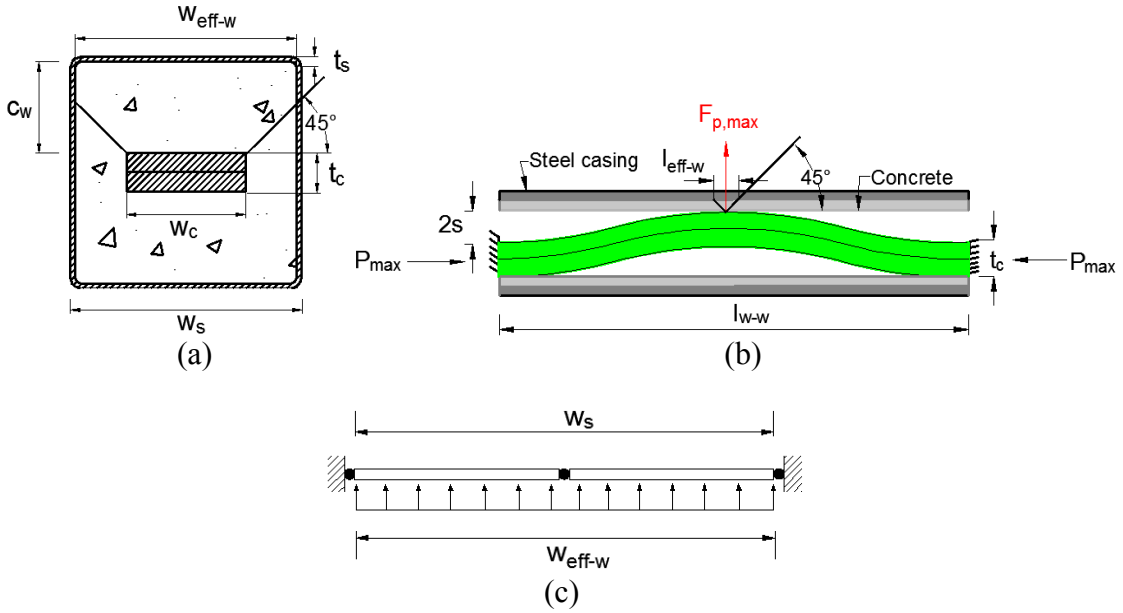

Fig. 11 - Effective inner surface for bulging due to weak-axis buckling: (a) width, (b) length; (c) equilibrium beam model

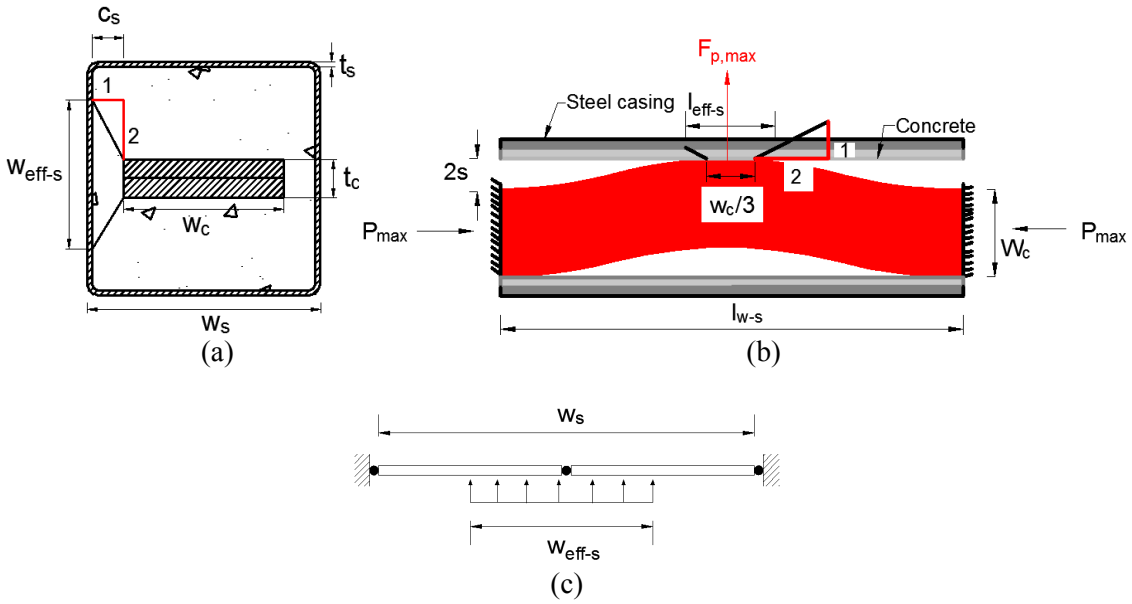

Fig. 12 - Effective inner surface for bulging due to strong-axis buckling: (a) width, (b) length; (c) equilibrium beam model

Table 4 - DCR for bulging failure of steel casing and minimum steel casing thickness

Test	P_{max} (kN)	t_c (mm)	w_c (mm)	w_s (mm)	w_{eff} (mm)	l_w (mm)	l_{eff} (mm)	t_s (mm)	*DCR*	Observed Failure
1	5671	51	235	305	165	1386	193	6.4	1.19	bulging
2	3874	51	159	305	305	605	241	6.4	1.02	bulging
3	3834	25	254	305	102	1499	161	6.4	1.02	bulging
4	2900	25	197	254	114	1161	155	6.4	0.81	none

7. Conclusions

Four full-scale new type buckling restrained braces (BRBs) were tested in this investigation; the BRBs differ from conventional ones in that they utilize straight steel core plates with two connection plates at each BRB end oriented perpendicular to the core. The following conclusions can be drawn:

(1) The new BRB configuration results in efficient use of steel and significant economy in manufacturing. Based on the fact that the two connection plates are perpendicular to the single or dual steel core plates, it is easier to build welded, pinned, or bolted connections. New type BRBs with similar total steel core area dissipated similar amounts of cumulative hysteretic energy to conventional BRBs.
(2) The hysteresis loops of the four full-scale BRBs exhibited repeatable and stable behavior with positive incremental stiffness; regardless of strong-axis or weak-axis buckling the new type BRBs met AISC 341 requirements. There was no rupture, brace instability, or brace end-connection failure up to displacements corresponding to 2% story drift and a strain in the core plates ranging from 3.2 to 4.2%. For each cycle reaching a deformation greater than the BRB yield displacement, the maximum tension and compression forces were greater than the nominal strength of the steel core; for all tests, the ratio of maximum compression to maximum tension force was less than 1.30.
(3) Occurrence of strong-axis or weak-axis buckling of the core plates was observed. The geometry of the casing and width of the core plate(s) determined the buckling direction. This behavior was predicted using the strut-and-tie model.
(4) A new definition for width and length of the effective inner surface for bulging failure of the steel casing was proposed for strong-axis buckling.
(5) Bulging failure of the steel casing observed in the tests was predicted using demand-to-capacity ratio (DCR) evaluations for both weak-axis and strong-axis buckling.

8. Acknowledgements

The authors acknowledge the financial support of Corebrace. The assistance of Mark Bryant of the University of Utah is also acknowledged.

9. References

[1] Uang CM, Nakashima M, Tsai KC (2004): Research and application of buckling-restrained braced frames. *Int. J. Steel Struct.,* **4** (4), 301–313.
[2] Usami T, Wang CL, Funayama J (2012): Developing high performance aluminum alloy buckling-restrained braces based on series of low-cycle fatigue tests. *Earthq. Eng. Struct. Dyn.,* **41** (4), 643–661.
[3] Black C, Makris N, Aiken I (2004): Component testing, seismic evaluation and characterization of buckling-restrained braces. *J. Struct. Eng.*, **130** (6), 880–894.
[4] El-Tawil S, Ekiz E (2009): Inhibiting steel brace buckling using carbon fiber-reinforced polymers: Large-scale tests. *J. Struct. Eng.*, **135** (5), 530–538.
[5] Rahaei AR, Alinia MM, Salehi SMF (2009): Cyclic performance of buckling restrained composite braces composed of selected materials. *Int. J. Civil Eng.*, **7** (1), 1-8.
[6] Genna F, Gelfi P (2012): Analysis of the lateral thrust in bolted steel buckling-restrained braces. I: Experimental and numerical results. *J. Struct. Eng.*, **138** (10), 1231–1243.
[7] Dusicka P, Tinker J (2013): Global restraint in ultra-lightweight buckling-restrained braces. *J. Compos. Constr.*, **17** (1), 139–150.
[8] Chou CC, Chen YC, Phan DH, Truong VM (2014): Steel braced frames with dual-core SCBs and sandwiched BRBs: Mechanics, modeling and seismic demands. *Eng. Struct.*, **72** (1), 26- 40.
[9] Wang C, Li T, Chen Q, Wu J, Ge H (2014): Experimental and theoretical studies on plastic torsional buckling of steel buckling-restrained braces. *Adv. in Struct. Eng.*, **17** (6), 871-880.
[10] Tremblay R, Bolduc P, Neville R, Devall R (2006): Seismic testing and performance of buckling-restrained bracing systems. *Canadian J. Civ. Eng.*, **33**, 183-198.

[11] Raddon BJ, Pantelides CP, Reaveley LD (2009): Full scale subassemblage testing of powercat series buckling-restrained brace. *Report No. CVEEN-09/1*, Dept. Civil and Env. Eng., Univ. of Utah, Salt Lake City, Utah, USA.
[12] Mirtaheri M, Gheidi A, Zandi AP, Alanjari P, Samani HR (2011): Experimental optimization studies on steel core lengths in buckling restrained braces. *J. Constr. Steel Res.*, **67** (8), 1244-1253.
[13] Miller DJ, Fahnestock LA, Eatherton MR (2012): Development and experimental validation of nickel-titanium shape memory alloy self-centering buckling-restrained brace. *Eng. Struct.*, **40**, 288-298.
[14] Palazzo G, Lopez-Almansa F, Cahís X, Crisafulli, F (2009): A low-tech dissipative buckling restrained brace: Design, analysis, production and testing. *Eng. Struct.*, **31** (9), 2152-2161.
[15] Ju YK, Kim MH, Kim J, Kim SD (2009): Component tests of buckling-restrained braces with unconstrained length. *Eng. Struct.*, **31** (2), 507-516.
[16] Wang CL, Usami T, Funayama J, Imase F (2013): Low-cycle fatigue testing of extruded aluminium alloy buckling-restrained braces. *Eng. Struct.*, **46**, 294-301.
[17] Mazzolani FM, Corte GD, D'Aniello M (2009): Experimental analysis of steel dissipative bracing systems for seismic upgrading. *J. Civil Eng. Mgmt.*, **15** (1), 7-19.
[18] Sun FF, Li GQ, Guo XK, Hu DZ, Hu BL (2011): Development of new-type buckling-restrained braces and their application in aseismic steel frameworks. *Adv. in Struct. Eng.*, **14** (4), 717-730.
[19] Zhao J, Wu B, Li W, Ou J (2014): Local buckling behavior of steel angle core members in buckling-restrained braces: Cyclic tests, theoretical analysis, and design recommendations. *Eng. Struct.*, **66**, 129-145.
[20] Lin PC, Tsai KC, Wang KJ, Yu YJ, Wei CY, Wu AC, Tsai CY, Lin CH, Chen JC, Schellenberg AH, Mahin SA, Roeder CW (2012): Seismic design and hybrid tests of a full-scale three-story buckling-restrained braced frame using welded end connections and thin profile. *Earthq. Eng. Struct. Dyn.,* **41**, 1001-1020.
[21] Chou CC, Chen SY (2010): Subassemblage tests and finite element analyses of sandwiched buckling-restrained braces. *Eng. Struct*., **32**, 2108-2121.
[22] Matsui R, Takeuchi T, Hajjar JF, Nishimoto K, Aiken I (2008): Local buckling restraint condistion for core plates in buckling restrained braces. *14WCEE*. Beijing, China.
[23] Wu AC, Lin PC, Tsai, KC (2012): A type of buckling restrained brace for convenient inspection and replacement. *15 WCEE*. Lisbon, Portugal.
[24] Zhao J, Wu, B, Li, W, Ou, J (2014): Local buckling behavior of steel angle core members in buckling-restrained braces: cyclic tests, theoretical analysis, and design recommendations. *Eng. Struct.,* **66**, 129-145
[25] Lin PC, Tsai, KC, Hsiao YY and Wu, AC (2014): Seismic tests of thin-profile buckling restrained braces. *10NCEE*. Alaska, USA
[26] Takeuchi T, Hajjar, JF, Matsui R, Nishimoto K, Aiken ID (2010): Local buckling restraint condition for core plates in buckling restrained braces. *J. Constr. Steel Res.*, **66** (2), 139-149.
[27] American Institute of Steel Construction (2010): Seismic provisions for structural steel buildings. *AISC 341-10*, Chicago, Ilinois, USA.
[28] Ansys Academic Research (2016), Release 17.1.
[29] American Concrete Institute (2014): Building code requirements for structural concrete and commentary. *ACI 318-14*, Farmington Hills, Michigan, USA.
[30] Xiao Y**,** Zhang Z**,** Hu J**,** Kunnath S**,** Guo P (2011): Seismic behavior of CFT column and steel pile footings *J. Bridge Eng*., **16**(5)**,** 575-586.
[31**]** Wu AC, Lin PC, Tsai KC (2014): High-mode buckling responses of buckling-restrained brace core plates. *Earthq. Eng. Struct. Dyn*., **43,** 375-393.